Journal of CO2 Utilization 67 (2023) 102337

Contents lists available at ScienceDirect

Journal of CO2 Utilization

journal homepage: www.elsevier.com/locate/jcou

A CO_2 valorization plant to produce light hydrocarbons: Kinetic model, process design and life cycle assessment

Tomás Cordero-Lanzac [a,*], Adrian Ramirez [b,1], Marta Cruz-Fernandez [c], Hans-Jörg Zander [d], Finn Joensen [e], Steven Woolass [c], Andreas Meiswinkel [d], Peter Styring [f], Jorge Gascon [b], Unni Olsbye [a,*]

[a] SMN Centre for Material Science and Nanotechnology, Department of Chemistry, University of Oslo, Sem Sælands vei 26, 0371 Oslo, Norway
[b] King Abdullah University of Science and Technology, KAUST Catalysis Center (KCC), Thuwal 23955, Saudi Arabia
[c] Tata Steel, Unit 2, Meadowhall Business Park, Carbrook Hall Road, Sheffield S9 2EQ, United Kingdom
[d] Linde GmbH, Dr.-Carl-von-Linde-Str. 6–14, Pullach 82049, Germany
[e] TOPSOE A/S, Kgs. Lyngby 2800, Denmark
[f] UK Centre for CO2 Utilization, Department of Chemical and Biological Engineering, The University of Sheffield, Sir Robert Hadfield Building, Sheffield S1 3JD, United Kingdom

ARTICLE INFO

Keywords:
Tandem catalyst
Kinetics
Reactor design
Process modeling
LCA

ABSTRACT

Reliable Life Cycle Assessment (LCA) of processes for valorization of CO_2-rich off-gas streams requires multi-disciplinary contributions that span the development of active and selective catalysts, reactor design, plant modeling and optimization, as well as environmental impact analysis. Herein, we present the design and study of a CO_2 valorization plant through methanol-mediated (tandem) hydrogenation to light hydrocarbons, with propane as the most abundant product. A state-of-the-art $PdZn/ZrO_2$ + SAPO-34 catalyst combination was screened for catalytic activity and selectivity in a wide operation range. Optimal process conditions were found at 350 °C, 30–40 bar and co-feeding of CO_2/CO. Kinetic parameters for the tandem reaction were extracted and used for the design of a multi-layer reactor, where the two catalysts are distributed according to: (i) CO_2-to-methanol catalyst; (ii) mixed catalyst bed, and; (iii) methanol-to-hydrocarbons catalyst. This configuration outperformed the conventional dual bed and mixed bed reactor configurations in terms of process design. A Life Cycle Assessment of the plant suggested that a substantial decrease in the global warming impact of propane production will be highly driven by using green hydrogen from either solar or wind sources, although the comparison with fossil-derived propane indicated already a reasonable improvement even when using grey hydrogen from natural gas.

1. Introduction

Increasing greenhouse gas (GHG) emissions, especially anthropogenic CO_2, is outpacing nature's carbon cycle, and has become an urgent threat to humankind because of the expected global warming, sea level rise or ocean acidification [1]. The Paris Agreement requires global CO_2 emissions to halve by 2030, reaching net zero by 2050, to limit the global warming below 2 °C [2,3]. On this matter, Carbon Capture and its Storage and Utilization (CCS and CCU) have emerged as key technologies in an attempt to mitigate the imminent global warming. Briefly, CCS technologies offer lasting mitigation of fossil-based CO_2 emission, while CCU technologies may replace fossil-based processes for producing fuels and chemicals, thereby reducing future CO_2 emissions [4,5] and contributing to a circular carbon economy [2].

Among the technologies for CO_2 utilization or valorization, thermocatalytic hydrogenation to methanol, methane or liquid fuels seem more promising. Kamkeng et al. [6] reviewed the state-of-the-art of most of these valorization routes and concluded that indeed CO_2 hydrogenation presents the highest feasibility for industrial implementation with a Technology Readiness Level (TRL) of 9 and the highest capability for net CO_2 used (1.0–2.6 ton CO_2 per ton of product). As the main drawback, CO_2 hydrogenation requires the highest utility consumption, and therefore the highest OPEX (operation expenses), which is mainly due to the highly energy-demanding pressurized H_2 [7]. A more specific study on green methanol production reported by Sarp et al. [8] indicates

* Corresponding authors.
E-mail addresses: t.c.lanzac@smn.uio.no (T. Cordero-Lanzac), unni.olsbye@kjemi.uio.no (U. Olsbye).
[1] Present address: Catalysis Hub, SwissCAT+ East, ETH Zürich, 8093 Zürich, Switzerland.

https://doi.org/10.1016/j.jcou.2022.102337
Received 20 October 2022; Received in revised form 16 November 2022; Accepted 18 November 2022
Available online 25 November 2022

Nomenclature

CCU	Carbon Capture and Utilization
E_j	apparent activation energy of each j step of the reaction network, J mol^{-1}
F, F_k	total molar flow rate through the reactor or through each control volume surface k, mol s^{-1}
GHG	greenhouse gases
GWP	global Warming Impact
h	enthalpy of a stream, J mol^{-1}
i	index for compounds
j	index for reaction steps
k	index for elements of the discretization
K_i	adsorption constant of each i compound, Pa^{-1}
K_j	equilibrium constant of each j step of the reaction network
k_j	kinetic constant of each j step of the reaction network
k^*_j	kinetic constant of each j step of the reaction network at the reference temperature
L	catalytic bed length, m
LCA	life cycle assessment
n_c, n_e	number of compounds and experiments, respectively
P_i	partial pressure of each i compound, Pa
P_z	total pressure in each z position of the reactor, Pa
Q_k	heat source in each k control volume, J s^{-1}
R	universal gas constant, J mol^{-1} K^{-1} or catalytic bed radius, m
RES	renewable sources of energy
r	catalytic bed radial position, m
r_j	reaction rate of each j step of the reaction network, mol kg^{-1} s^{-1}
S	reactor cross-section, m^2
T^*	reference temperature, 623 K
y_i, y_i^e	calculated and experimental molar fraction of each i compound, respectively
z	catalytic bed axial position, m
∇T	temperature gradient in the axial or radial position, K m^{-1}
δSk	section of each k control volume, m^2
δVk	volume of the control volume k, m^3
δz	length of each k control volume, m
$\lambda_{eff,k}$	thermal conductivity through the control volume surface k, J m^{-1} K^{-1} s^{-1}
ν_{ij}	stoichiometric coefficient of each i compound in each j reaction step
ρ	bed density, kg, m^{-3}
ω_i	weight factor considered for each i compound

that at least 89% of the energy required for CO_2 hydrogenation will be used for H_2 production by water splitting. These authors demonstrated that CO_2 hydrogenation and CO_2 electrolysis could produce methanol with a similar energy use to that needed in the current process from natural gas (around 12 kWh per kg of MeOH) with negative Net GHG emission of ca. − 0.77 kg CO_2 equivalents per kg MeOH (assuming all renewable energy sources). The main parameters that seem generally accepted in the wide literature are the necessity of coupling CO_2 valorization technologies with renewable energy sources (RES) [6–12] and the leading position of CO_2 thermocatalytic hydrogenation among the other technologies for large-scale implementation. In fact, Carbon Recycling International was a pioneer in the field, and commercialized in 2012 the so-called George Olah renewable methanol plant in Iceland [13]. This plant uses large-scale water electrolysis and achieves a methanol production of 4 kton per year with CO_2 recycling capacity of 5.5 kton per year using geothermal energy.

Industrial CO_2 hydrogenation has generated much attention in the research community in the last years, with an increasing number of works studying the CO_2-to-methanol process, plant design, techno-economic and life cycle assessments (LCA). Most of the work has been done within the boundaries of the CO_2 hydrogenation plant, performing optimizations of the process parameters [14], estimations of the maxima CO_2 abated [15], or required costs (methanol and H_2 price or CO_2 tax) to make a green methanol plant affordable [16–19]. Khojasteh-Salkuyeh et al. [20] performed a more specific study on the thermal efficiency of methanol production plants, and concluded that CO_2 hydrogenation can produce methanol more efficiently than dry reforming (48% vs 41% LHV) but still far from the conventional route (autothermal or steam reforming of methane) (68%). Nevertheless, their LCA suggested that CO_2 net zero emissions will be only achieved with very low electricity GHG intensity, making necessary the use of RES, especially for H_2 production. For this reason, an increasing number of studies are now extending the boundaries of the studies to technologies for carbon capture and H_2 production [10,12,21], to the comparison of different sources of water splitting [11] or to purely the analysis of H_2 cost for making CO_2 valorization cheaper [1]. But this factor may have overshadowed the most recent advances on catalytic systems for CO_2 hydrogenation, as most of the work is done using kinetic models for the classic Cu-ZnO-Al_2O_3 catalyst, which performance is inferior to most state-of-the-art catalysts [22]. This is understandable because it requires a multidisciplinary effort to extract kinetic models from homemade catalysts under realistic reactor conditions and implement them into plant design models [7].

In the last decade, substantial research has been devoted to seek out new promising catalysts for converting CO_2 and H_2 to methanol. Among them, metal oxides and mixed metal oxides stand out [23–26]. Furthermore, main effort is now focused on the *in situ* transformation of the formed methanol to hydrocarbons by adding an acidic catalyst in a direct process from the abated CO_2 to chemicals or fuels. Although the optimization of reaction conditions for this tandem approach is challenging, the combination of these metal oxides with SAPO-34 (the commercial methanol-to-olefins catalyst) has provided encouraging results. Different authors have systematically reported increases in CO_2 conversion with respect to the methanol synthesis, negligible deactivation by coking of the zeotype, light hydrocarbons selectivities above 60% and a significant mitigation of CO and methane production per pass [27–29]. In a previous contribution, we reported the superior catalytic performance of the combination of a PdZn/ZrO_2 oxide with SAPO-34, obtaining CO_2 conversion of 40%, selectivity to C_2-C_4 hydrocarbons of 73% and excellent catalyst stability [30]. The encouraging results inspired us to translate these notable advances to the design of a CO_2 valorization plant for evaluating their impact by developing kinetic models for these specific catalytic systems.

Ab initio computation has played a big role for the development of state-of-the-art catalysts [23,25,31]. However, the integration of *ab initio*-based kinetics with reactor design models makes the mathematical problem too complex to incorporate into a plant simulation [32]. Simplifications of microkinetic models have been proposed with the aim of reproducing experimental observations of product distribution [33], but lumped macrokinetic models based on reactor performance are the optimal approach to design and simulate reactors [34–36]. Herein, we present a kinetic model that efficiently predicts the performance of our previously introduced PdZn/ZrO_2 + SAPO-34 catalyst. The model has been applied for the design of a multi-layer packed bed reactor. Different to the two-stage approach (CO_2 to methanol + methanol to hydrocarbons in different reactors), here we take advantage of the *in situ* reaction of methanol to shift CO_2/methanol equilibrium in the main layer of the reactor, while avoiding temperature runaways at the entrance of the

reactor with a PdZn/ZrO_2 layer and methanol downstream with a pure SAPO-34 layer. To these operating advantages, the clear benefit of operating in one unit and the potential savings in reactor cooling are also worth of mentioning. The multi-layer reactor system was then implemented in a simulation model of a CO_2 hydrogenation plant to directly produce hydrocarbons, a strategy barely studied in literature at process design scale. The potential performance of the plant has been analyzed including the main environmental impacts by means of LCA. These impacts have been compared to the estimated environmental cost of producing propane at a refinery from crude oil, suggesting improvements in most of the analyzed categories.

2. Methodology

2.1. Experimental runs

CO_2 hydrogenation experiments were carried out in a packed bed reactor using a physical mixture of PdZn/ZrO_2 catalyst and commercial SAPO-34 (ACS materials). Briefly, the PdZn/ZrO_2 catalyst was prepared by adding 10 g of Zirconium(IV) oxide (Merck) to a solution of 3.4 g Zn$(NO_3)\cdot 6\,H_2O$ (Merck) and 0.33 g $Pd(NO_3)_2$ (Merck) in 7 ml of water. The mixture was stirred for about 15 min, and then evaporated under stirring at 65 °C. Afterwards, the material was dried at 200 °C for 1 h and calcined at 500 °C for 5 h. The calcined catalyst was reduced for 1 h in hydrogen at 400 °C (ramp 5 °C min^{-1}), to form the active PdZn alloy species, and finally passivated at room temperature in 1% O_2 in N_2 to stabilize the active function. More details on catalyst synthesis and characterization can be found elsewhere [30].

The PdZn/ZrO_2 catalyst and SAPO-34 were pelletized together in a 1/1 mass ratio and sieved to a particle size of 150–250 μm. The catalytic tests were carried out in a sixteen channel Flowrence test rig from Avantium, provided with a membrane-based pressure controller and mass flow controllers for inert and reactant gas feeds. Prior to reaction, the samples were pretreated *in situ* in the reactor under a 10%H_2 (in inert) continuous flow at 400 °C for 4 h, to remove water and adsorbed species from SAPO-34 pores and ensure the state of the active PdZn alloy species. Then, reactors were pressurized and each group of four reactors was set to a different reaction temperature before the reactant mixture consisting of H_2, CO_2, CO and He as internal standard was fed into the sixteen reactors. In all cases, one of the reactors in each group of four was used without catalyst as a blank. A wide range of operating conditions was tested in order to develop the kinetic model, with the central point of the experimental design being 350 °C and 40 bar. Altogether, 46 different sets of conditions were tested with at least three repetitions under the following conditions: temperature of 325–400 °C; pressure of 20–50 bar; GHSV of 1500–24000 $cm^3\,h^{-1}\,g^{-1}$; H_2/CO_x of 3, CO_2/CO_x of 1, 0.5 and 0 (with CO_x being CO_2 + CO) and time on stream 12 h.

Reaction products were analyzed online in a Gas Chromatograph (Agilent 7890B) provided with three detectors, a TCD and two FIDs. The TCD was equipped with two Haysep precolumns and a MS5A column for separation of He, H_2, CH_4, CO_2 and CO. FIDs were equipped with Gaspro and an Innowax columns for the separation of C_1–C_8 hydrocarbons and DME, and oxygenates and aromatics, respectively. Reactions were monitored by conversion and selectivity indexes, which are defined in the **Section S1** of Supplementary Material.

2.2. Kinetic model methodology

The kinetic model for the tandem conversion of CO_2 to light hydrocarbons was developed by using the convection-dispersion-reaction equation for each compound in the reaction medium. Due to the reactor characteristics, isobaric and isothermal conditions were assumed (reactor diameter of 2 mm and less than 5 cm bed height). Moreover, pure convective transport was assumed, with negligible radial dispersion due to the small diameter of the reactor, and negligible axial dispersion, with Re values of ca. 10^5 at the used flow conditions. Deactivation was not observed during long-time experiments and after the catalyst pretreatment in H_2 and the first hours of reaction, steady state was reached (see details in the Section 3.1). With this assumption, the reactor can be modeled using the steady-state design equation for a packed bed reactor. Then, the molar fraction of each *i* compound (y_i) can be expressed as

$$\frac{1}{S}\frac{d(Fy_i)}{dz} = \rho\sum_j \nu_{ij}\, r_j \tag{1}$$

for a catalytic bed length $0 < z < L$, where *S* is the reactor cross-section, *F* is the total molar flow rate, ρ is the bed density, ν_{ij} is the stoichiometric coefficient of each *i* compound in each *j* step of the reaction network and r_j is the reaction rate of each *j* step of the reaction network, described by the reactions occurring through interaction with both functions of the catalyst: Hydrogenation on the metal alloy/oxide and MTH chemistry on the SAPO-34:

$$CO_2 + 3H_2 \rightleftarrows^{1} CH_3OH + H_2O \tag{2}$$

$$CO_2 + H_2 \rightleftarrows^{2} CO + H_2O \tag{3}$$

$$CO + 2H_2 \rightleftarrows^{3} CH_3OH \tag{4}$$

$$CO + 3H_2 \longrightarrow^{4} CH_4 + H_2O \tag{5}$$

$$2CH_3OH + H_2 \longrightarrow^{5} C_2H_6 + 2H_2O \tag{6}$$

$$3CH_3OH + H_2 \longrightarrow^{6} C_3H_8 + 3H_2O \tag{7}$$

$$4CH_3OH + H_2 \longrightarrow^{7} C_4H_{10} + 4H_2O \tag{8}$$

On the metal alloy/oxide function, the following reactions were considered: CO_2 hydrogenation to methanol (reaction 1, Eq. (2)), reverse water-gas shift (reaction 2, Eq. (3)), CO hydrogenation to methanol (reaction 3, Eq. (4)) and the undesired formation of methane from CO (reaction 4, Eq. (5)). On the other hand, methanol conversion to ethylene, propylene and butenes was assumed to proceed over the SAPO-34 [37]. Nevertheless, our previous observations suggest that the presence of high partial pressure of H_2 and this Pd-containing catalyst led to fast hydrogenation of unsaturated hydrocarbons to ethane, propane and butanes [30], thereby contributing to reactions 5–7 (Eqs. (6)–(8)).

Reaction rates (r_j) are defined by Langmuir-Hinshelwood equations

$$r_1 = \frac{k_1\left(P_{CO_2}P_{H_2}^3 - \frac{P_{CH_3OH}P_{H_2O}}{K_1}\right)}{\left(1 + K_{CO_2}P_{CO_2} + \sqrt{K_{H_2}P_{H_2}}\right)^2} \tag{9}$$

$$r_2 = \frac{k_2\left(P_{CO_2}P_{H_2} - \frac{P_{CO}P_{H_2O}}{K_2}\right)}{\left(1 + K_{CO_2}P_{CO_2} + \sqrt{K_{H_2}P_{H_2}}\right)^2} \tag{10}$$

$$r_3 = \frac{k_3\left(P_{CO}P_{H_2}^2 - \frac{P_{CH_3OH}}{K_3}\right)}{\left(1 + K_{CO_2}P_{CO_2} + \sqrt{K_{H_2}P_{H_2}}\right)^2} \tag{11}$$

$$r_4 = \frac{k_4P_{CO}P_{H_2}}{\left(1 + K_{CO_2}P_{CO_2} + \sqrt{K_{H_2}P_{H_2}}\right)^2} \tag{12}$$

$$r_5 = \frac{k_5P_{CH_3OH}}{1 + K_{H_2O}P_{H_2O}} \tag{13}$$

$$r_6 = \frac{k_6P_{CH_3OH}}{1 + K_{H_2O}P_{H_2O}} \tag{14}$$

$$r_7 = \frac{k_7P_{CH_3OH}}{1 + K_{H_2O}P_{H_2O}} \tag{15}$$

where k_j is the kinetic constant of each j step of the reaction network (Eqs. (2)–(8)), K_j is the equilibrium constant of each j step, P_i is the partial pressure of each i compound and K_i is the adsorption constant of each compound (CO_2, H_2 and water). For those hydrogenation reactions that take place on the metal alloy/oxide, the adsorption of CO_2 and the dissociative adsorption of H_2 were considered in a single site as no significant improvement was observed by Ghosh et al. [38] when two different sites were considered. The equilibria of the first three reactions are considered using the empirical correlations with temperature proposed by Iluita et al. [39] (detailed in **Section S2** of Supplementary Material), and kinetic constants (k_j) are defined with a reparameterized form of the Arrhenius equation

$$k_j = k_j^* \exp\left[-\frac{E_j}{R}\left(\frac{1}{T}-\frac{1}{T^*}\right)\right], \tag{16}$$

where k^*_j is the kinetic constant of each j step of the reaction network at the reference temperature T^* (623 K), E_j is the apparent activation energy of each j step of the reaction network and R is the universal gas constant.

The system of partial differential equations was transformed into a system of ordinary equations and solved using a finite-difference discretization method and a Runge-Kutta method of orders 1–5. Detailed conservation equations and boundary conditions can be found in **Section S2** of Supplementary Material. The reactor model was solved by iterative computation to optimize the k^*_j, E_j and K_i parameters. For that, an objective function to be minimized was defined based on the sum of square errors (SSE) between calculated and experimental data

$$SSE = \sum_{i=1}^{n_c} \omega_i \sum_{n=1}^{n_e} \left(y_i - y_i^e\right)_n^2, \tag{17}$$

where y_i and y_i^e are the calculated and experimental molar fractions of each i compound, respectively, ω_i is the weight factor considered for each i compound and n_c and n_e are the number of compounds and experiments, respectively.

2.3. CO_2 valorization plant design

A CO_2 valorization plant to produce light hydrocarbons was designed and simulated using the computed kinetics from experimental data. The core part of the plant is the reactor, which, like our experimental setup, consists of a packed bed reactor. In this case, the numerical implementation of the reactor model does not only solve the pseudo-homogeneous conservation equations of mass, but also of energy and momentum. Due to the upscaling of the reactor volume, the discretization scheme used is based on a finite volume method, accounting for the axial and radial directions, which provides a non-linear equation system (assuming steady-state conditions), numerically solved using a Newton solver. Then, for each k infinitesimal control volumes:

$$\sum_k F_k\, y_i + \delta V_k\, \rho \sum_j \nu_{ij}\, r_j = 0 \tag{18}$$

$$\sum_k F_k\, h - \sum_k \lambda_{eff,k} \nabla T\, \delta S_k + Q_k = 0 \tag{19}$$

$$P_z - P_{z-\delta z} = \frac{dP}{dz}\delta z \tag{20}$$

defined for axial positions $0 < z < L$, radial positions $0 < r < R$, and where F_k is the total flow rate through the control volume surface k, δV_k is the volume of the control volume k, h is the enthalpy of the F_k stream and depends on its composition and temperature, $\lambda_{eff,k}$ is the thermal conductivity through the control volume surface k, ∇T is the temperature gradient in the axial or radial position, δS_k is the section of each k control volume, Q_k is the heat source in each k control volume, P_z is the pressure in each z position of the reactor, δz is the length of each k control volume and the pressure derivative with respect to the position is considered a function of the linear velocity, density and viscosity of the fluid stream. Reaction rates (r_j) are those calculated from our kinetic model and considering spherical or close to spherical particles, correlations for radial bed conductivity and the wall heat transfer coefficient (λ_{eff}) are available in the literature [40]. Detailed conservation equations and boundary conditions for this three-dimensional reactor model can be found in **Section S2** of Supplementary Material.

The in-house programmed reactor was integrated into the process simulation plant detailed in Fig. 1, designed and simulated using UniSim® R480 (Honeywell®). The CO_2 valorization plant consists of three stages: Compression stage, reaction stage and separation stages. CO_2 and H_2 are the two main feeds to the plant, considered to be produced in external facilities (see below). Feeds were considered at standard conditions of temperature and pressure and compressed using isentropic compressors with adiabatic efficiencies of 75% (A in Fig. 1). Compressed feed mixture is then heated to the reaction temperature and mixed with the recirculated stream before they are sent to the reactor. Reactor model was simulated using the kinetic model developed from experimental data and a three-layer design detailed below (B in Fig. 1). Downstream to the reactor, the outlet stream is condensed (C in Fig. 1), leading to the recirculation stream (uncondensed stream), an organic hydrocarbon phase (including the main products) and an aqueous phase. The condensation temperature is limited by ice formation to > 0 °C but should be as low as possible to achieve the best possible condensation. Light species like methane, which are formed in undesired side reactions, are recycled to the reactor together with unconverted H_2/CO_2/CO gas and tend to accumulate in the gas recycle. To remove these species from the gas recycle loop, a gas purge is required. The purge rate depends on the feed stream purities as well as on the reaction conversion and selectivities. For our pure reactant stream, a purge ratio of 1 wt% was considered. The hydrocarbon phase from the decanter as well as the gas purge are first dried (D and E in Fig. 1) and rectified (F in Fig. 1). Under dry conditions, no ice can be formed and the condenser temperature can be reduced below 0 °C. A lower condenser temperature improves the product recovery. A good separation is achieved at ca. − 20 °C. Rectification is required in order to separate C_{3+} hydrocarbons from light gases (F in Fig. 1). An improvement of ethane separation will require extra separation stages and more expensive operations, which is out of the scope of the current study. The overhead product of the rectification column is a gas mixture with condenser temperature dew point, avoiding further condensate at the available temperature.

For the steady-state simulation of the plant, NRTL (Nom-Random Two Liquid) model was used for the calculation of the activity coefficient on the liquid phase, and SRK (Soave-Redlich-Kwong) equation of state was used for the vapor model [41]. Inside the UniSim® environment, convergence and mass balance closure were achieved by a Modified Inside-Out algorithm with adaptive damping factor [42]. The reactor and plant model simulations were decoupled to avoid inconsistencies related to the mass balances due to the different tolerance levels required to converge each model. From computation level, process simulation defines reactor feed, whereas the reactor model provides the process model with the outlet product stream. To optimize computation time and accuracy, a conversion reactor was applied on the process model level, with conversions calculated by the three-layer reactor model. Starting with an initial guess, only a few iterations were required to converge both models.

The plant was simulated for a target valorization of 100 kg h^{-1} of pure CO_2, which corresponds to an approximate capacity of ca 700 ton CO_2 y^{-1}. The H_2 stream was adjusted to provide stoichiometric ratio in the reactor feed. This optimizes the maximum allowed equilibrium limitation and maximizes the plant operation potential due to the severe restriction of the process. For an overall process reaction where CO_2 is aimed to be converted to propane (even considering ethane and butane the average carbon number of the products is close to 3), a

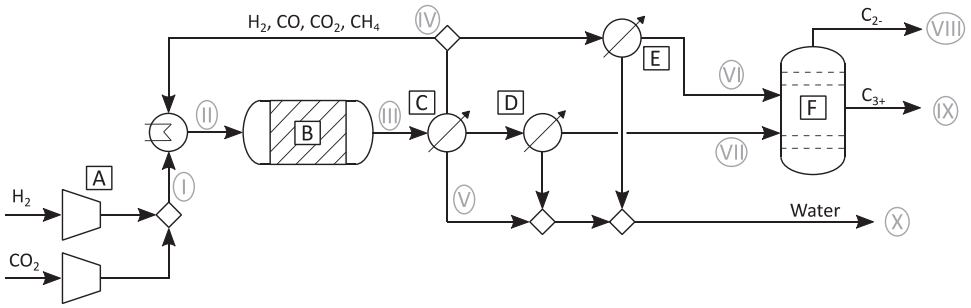

Fig. 1. Overall scheme of the simulated CO_2 valorization plant to produce light hydrocarbons. A: Compression stage; B: Multi-layer packed bed reactor; C: 3-phase separation; D: Liquid phase dryer; E: gas phase dryer; F: Rectification.

stoichiometric ratio of $H_2/CO_2 = 10/3$ (a bit higher than experimental values) will maximize the allowed equilibrium conversion, and was the used feed ratio in our simulations.

2.4. Life cycle assessment

A Life Cycle Assessment (LCA) of the simulated plant was carried out to assess whether the use of CO_2 containing process gases from industry in the carbon capture and utilization (CCU) process for producing propane would have a positive environmental impact, when compared to the conventional production of propane and use of the process gases. The gate-to-gate LCA study was based on the process design of the CO_2 valorization plant. Two scenarios were considered, a baseline scenario and a CCU scenario (Fig. 2a). Fig. 2b details the LCA system boundaries. In the baseline scenario, propane is produced at a refinery from fossil sources. In the CCU scenario, the system boundary considers the CO_2 containing process gas as input and includes the CO_2 valorization plant and additional processes needed to produce CO_2-based propane, such as hydrogen production. The purification of the CO_2 source or the effect of impurities on the process kinetics were not considered and are out of the scope of this work. As this process gas usually contains a small amount of hydrogen (2.7 vol%), this was deducted from the hydrogen requirements at the plant. All assumption for the studies are detailed in **Section S6** of the Supplementary Material.

The impact of the CO_2 valorization plant was evaluated at different deployment timelines, by assuming different average European grid electricity mixes (Table S3). The choice of electricity mix has an impact on the Global Warming Potential (GWP) impact of the CO_2 valorization plant. This is linked to the compression of the input hydrogen and CO_2, and to the purge gas (a mix of C_1-C_2 products). The purge gas is assumed to be combusted to produce electricity, which reduces the need to generate electricity from the grid. This electricity receives a GWP credit proportional to the GWP impact of the electricity mix. The wastewater generated in the plant is assumed to be sent for municipal wastewater treatment.

For the LCA study, a model was created to represent the CO_2 valorization plant using the LCA software GaBi. A functional unit was defined to allow an accurate comparison between the baseline case and the CCU scenario. A functional unit of 1 kg of propane was chosen (Fig. 2b), as this is the most abundant hydrocarbon in the product stream (Table S2, 81% propane, 19% butane). An alternative functional unit could have been LPG, as the chemical composition is similar to that of the CO_2 valorization plant product. Neither propane nor LPG have specific production lines, so the environmental impacts are estimated based on allocation methodologies from the overall environmental impacts of the production process. Additionally, LPG is an intermediate product, whereas propane is considered a final product with more defined markets and uses. For these reasons, a functional unit of 1 kg of propane was chosen. In LCA methodology, to estimate the environmental impact in processes that produce more than one product, different allocation methods can be used to divide the overall environmental impact of a process between the different products (and by-products). In this case, for the environmental impact of propane, we used a database from Sphera that uses allocation by mass and net calorific value. The inventory data for propane production from crude oil covered the entire supply chain of the refinery products, including well drilling, crude oil production and processing and transportation.

The main impact category considered was the Global Warming Potential (GWP), but four mid-point indicators were also evaluated: Abiotic Depletion (ADP), Acidification Potential (AP), Eutrophication Potential (EP) and Photochemical Ozone Creation Potential (POCP). The definition of these indicators and databases for this study are detailed in **Section S6** of the Supplementary Material. The characterization factors for transforming inventory data into impact assessments were based on CML 2001 methods. The method used is CML 2001 updated in January 2016, as this methodology is used by the *International Environmental*

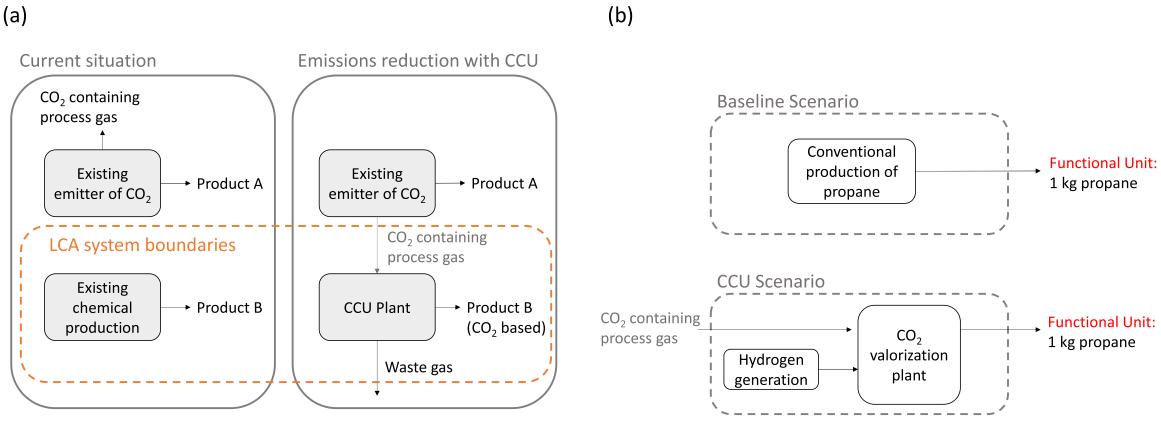

Fig. 2. (a) Life Cycle Assessment scenarios and (b) system boundaries.

Product Declaration (EPD) System [43], as a default for product category rules, and is advised in the *TEA and LCA guidelines for CCU* [44].

3. Results and discussion

3.1. Kinetic model and experimental data fitting

The kinetics of CO_2 hydrogenation over the $PdZn/ZrO_2$ catalyst mixed with SAPO-34 was studied in a packed bed reactor in a wide range of operating conditions to obtain reliable development and fitting of the kinetic model. Experimental runs were designed accounting for the optimal conditions for this catalyst, which was in-depth studied in our previous work [30]. From that, we observed that a minimum temperature of 350 °C was necessary to activate the *hydrocarbon pool* mechanism to convert methanol into hydrocarbons. In addition, with the overall plant design in mind, the separation of the most abundant hydrocarbons in the effluent would be difficult above their critical pressure (ethane, ca. 48.7 bar and propane, ca. 42.5 bar). For those reasons, 350 °C and 30–40 bar were selected as the optimal operation conditions of the plant. A set of reactions at conditions surrounding the central point of the experimental design was carried out, and different gas hourly space velocity (GHSV) values were tested at any given conditions. Due to the necessity of recirculation in this kind of chemical process, the difficulty of CO_2/CO separation and the observed catalytic activity for CO hydrogenation, experiments with CO_2/CO co-feeds and pure CO were also evaluated. Table S1 summarizes all tested conditions also including CO_x conversion (CO_2 + CO, see index definition in **Section S1** of the Supplementary Material).

Fig. 3 shows an evaluation of the effect of the main reaction variables on the catalytic performance. Fig. 3a illustrates the effect of temperature on conversion, CO selectivity and hydrocarbon distribution. Please note that CO_x conversion is lower than CO_2 conversion (hollow vs solid symbols in Fig. 3) because CO is considered as unreacted feed. CO_2 conversion increases from 325 to 350 °C, reaching a plateau at higher temperatures. Nonetheless, regarding the evolution of CO_x conversion and CO selectivity, this behavior is caused by a promoted formation of CO through the reverse water gas-shift reaction. This is a known endothermic reaction (ΔH_{298}, 41 kJ mol^{-1}), therefore favored at high temperatures. Otherwise, hydrogenation of both CO_2 and CO to methanol is exothermic (ΔH_{298}, −49.5 and −92 kJ mol^{-1}, respectively [5]), which promotes the production of methanol at the lowest possible temperature. Regarding the hydrocarbon distribution of Fig. 3, C_3 is the main fraction at all conditions. It is worth noting that all observed hydrocarbons are paraffins because of the ability of the Pd-containing system to hydrogenate olefins [30]. Methane production over the hydrogenating catalyst is also increased with temperature, where the rates of all reactions are promoted. Methane is another C_1 product that should be avoided due to separation restrictions.

The effect of total pressure on reaction parameters is shown in Fig. 3b. As expected by the stoichiometry of the reaction (Eqs. (2) and (4)), CO_2 conversion increases with total pressure, which is very noticeable from 20 to 30 bar. Here, CO_x conversion increases following the same tendency to that of CO_2 conversion, with CO selectivity being maximum at 30 bar (ca. 60%). Methane selectivity is roughly constant in the studied pressure range and C_2 selectivity significantly decreases upon increasing pressure leading to a promotion of C_3 selectivity. This behavior was previously ascribed to an inhibition of polymethylbenzene dealkylation (unimolecular reaction and the main source of ethylene) during the MTH reaction at high pressure [45].

Co-feeding CO in a 50 vol% mixture with CO_2 or reactions with pure CO lead to a CO_x conversion increase from 11.5% (Figs. 3b) to 16.2% and 18.3%, respectively, at 350 °C and 30 bar (Fig. 3c). Hydrocarbon distribution is very similar with a slight increase in methane selectivity. This suggests that it should be mainly produced from CO (Eq. (5)). At 400 °C and 40 bar, this behavior is even more noticeable. CO_x conversion increases from 8.3 (Fig. 3a) to 37.5% (Fig. 3c) with a methane selectivity (among hydrocarbons) up to 15.5%. The higher difference at 400 °C is mainly due to the higher thermodynamics constraints of CO_2 hydrogenation *vs* CO hydrogenation. This, along with the high productivity of methane, makes this temperature unfeasible from an operation point of view. For all these reasons, 350 °C should be considered as the optimum operating temperature for the process. As an unequivocal metric of reactor performance, the yield of liquefied petroleum gases (LPG, product of interest C_2-C_4) is defined in **Section S1** of the Supplementary Material, and plotted in Fig. S1 at the previously discussed conditions of the experiments in Fig. 3. LPG production is maximized at 350 °C, 50 bar and feeding CO (Fig. S1).

All results derived from experiments at the conditions highlighted in Table S1 were used for the development of the steady-state kinetic model. The $PdZn/ZrO_2$ + SAPO-34 catalyst combination showed a fairly stable performance during CO_2 hydrogenation to hydrocarbons. Although one could have expected deactivation by coking due to the nature of MTH reaction, our previous observations suggested that it does not affect catalyst activity in a great extent at the targeted conditions here [30]. Moreover, regeneration cycles were carried out, even in those cases where deactivation was not observed, to ensure the stability of the catalyst after the thermal treatment. Raman spectroscopy indicated the incipient formation of coke after reaction with a total content of coke lower than 4 wt% (*ex situ* measurements after reaction). Furthermore, significant changes were not observed in the $PdZn/ZrO_2$ catalyst function after the reactions, meaning that sintering or migration of metallic component can be neglected as a source of deactivation as well. As an

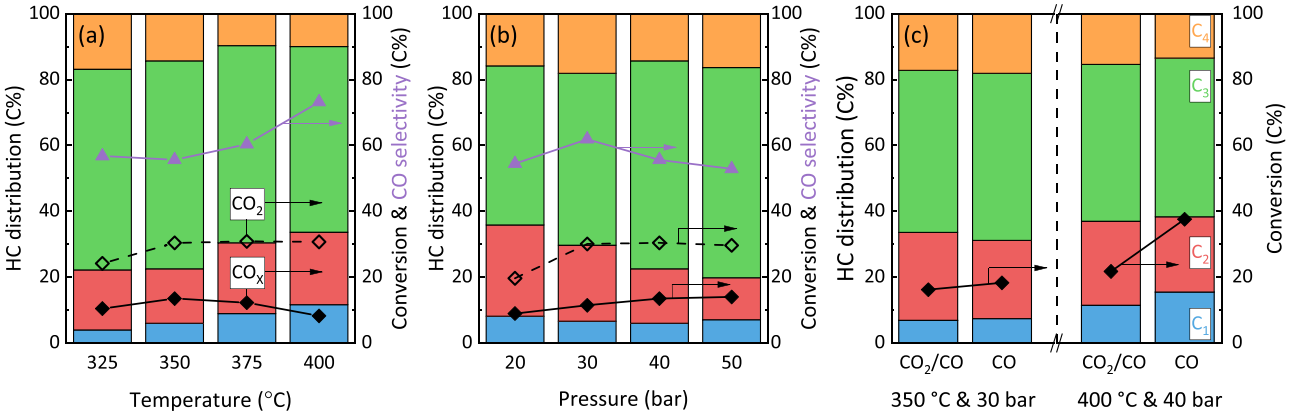

Fig. 3. Effect of (a) temperature (at 40 bar) and (b) total pressure (at 350 °C) on CO_2 and CO_x conversion, CO selectivity and hydrocarbon distribution. (c) CO_x conversion and hydrocarbon distribution for CO_2/CO co-feed and CO hydrogenation at selected temperatures and pressures. GHSV = 3000 cm^3 h^{-1} g^{-1}, H_2/CO_x = 3/1.

example, Fig. S2 shows the stable evolution with time during 72 h (at the central experimental conditions: 350 °C and 40 bar) achieved by this catalytic system after a short initial stabilization.

The above-introduced model was used and after experimental data fitting, the optimal parameters that minimized the objective function (Eq. 17) are summarized in Table 1. The deviations of the parameters (95% confidence intervals) were estimated from the discrepancies between experimental data and model accuracy. Kinetic parameters and adsorption constants were in the range of previous studies [7,30], and apparent activation energies are also similar to those reported by other groups in similar systems [38]. Please note that in most experimental results, CO_2-to-methanol reaction (Eq. 2) is in equilibrium (see below) aiming at maximum CO_2 and CO_x conversion. This fact decreased the accuracy of individual step kinetics computation. For this reason, the estimated deviation for k_1 is high and the computation of a reliable apparent activation energy was not possible. Recently, Lacerda de Oliveira et al. [33] proposed a kinetic model for CO_x hydrogenation at different levels of refinement using as a base a microkinetic model derived from DFT calculations. Herein, we have used their value of apparent activation energy as a starting guess and a small refinement of the parameter was performed due to the differences in the catalytic system. Besides, the best fitting of methane concentration was found without considering reversible reaction and assuming order 1 for CO and H_2 instead of considering the stoichiometry of the reaction. This was due to the low extent of this reaction in most cases and the difference in methane productivity between reactions with CO_2 or CO in the feed (significantly higher for the latter). Regarding hydrocarbon production, the primary products derived from MTH chemistry are C_2, C_3 and C_4 olefins, which are rapidly hydrogenated to paraffins and cannot be properly quantified experimentally. To maintain the level of significance, only one apparent activation energy, common for *hydrocarbon pool* mechanism reactions, was considered. The value of this energy was estimated to be ca. 84 kJ mol^{-1}, higher than most of the metal alloy/-oxide function-related reactions (reactions 2–4. Eqs. (3)–(5)), but lower than the activation of CO_2-to-methanol reaction.

Fig. 4a and b show a comparison between calculated and experimental data under the most relevant operating conditions: 350 °C and 30 bar (Fig. 4a) or 40 bar (Fig. 4b) for pure CO_2 feed (central point of the experimental design). As observed, the evolution with space time of the C-containing products is well predicted by the model. In both cases, CO_2 simulated conversion match our experimental observations, and the main secondary product is CO. As representative of hydrocarbons, the C_3 fraction, which is most abundant, continuously increases with space time. An individual analysis of CO reactivity is required for the computation of CO hydrogenation to methanol (reaction 3, Eq. (4)) and its mathematical decoupling from methanol formation *via* WGS (reverse reaction 2, Eq. (3)) plus CO_2 to methanol (reaction 1, Eq. (2)) reactions. As illustrated in Fig. 4c, our model is also able to predict CO tandem hydrogenation to hydrocarbons at different conditions: CO/CO_2 co-feed at optimal process conditions (solid symbols and continuous line); CO hydrogenation at optimal process conditions (hollow symbols and dashed lines) and; CO hydrogenation at the harshest tested conditions (crossed symbols and double lines). In those experiments, the evolution with space time of CO conversion, CO_2 formation *via* WGS (reverse reaction 2, Eq. (3)) and hydrocarbon formation *via hydrocarbon pool* is followed by the model. As an overview of the overall fitting, a parity plot between experimental and calculated data is shown in Fig. S3 and the fitting of all individual data matrices in Table S1 can be found in Figs. S4 and S5.

Table 1
Calculated kinetic parameters and adsorption constants for the kinetic model in Eqs. (9)–(15).

	k^*	E
		(kJ/mol)
k_1 (mol g^{-1} h^{-1} bar^{-4})	$(8.35 \pm 6.81)10^{-6}$	$(1.04 \pm 0.80)10^{2}$ [a]
k_2 (mol g^{-1} h^{-1} bar^{-2})	$(4.49 \pm 0.48)10^{-4}$	$(4.91 \pm 1.40)10^{1}$
k_3 (mol g^{-1} h^{-1} bar^{-3})	$(1.32 \pm 0.23)10^{-5}$	$(5.97 \pm 1.71)10^{1}$
k_4 (mol g^{-1} h^{-1} bar^{-2})	$(9.11 \pm 0.51)10^{-6}$	$(4.55 \pm 1.84)10^{1}$
k_5 (mol g^{-1} h^{-1} bar^{-1})	$(3.14 \pm 0.47)10^{-2}$	$(8.38 \pm 1.17)10^{1}$
k_6 (mol g^{-1} h^{-1} bar^{-1})	$(4.21 \pm 0.59)10^{-2}$	$(8.38 \pm 1.17)10^{1}$
k_7 (mol g^{-1} h^{-1} bar^{-1})	$(9.11 \pm 0.23)10^{-3}$	$(8.38 \pm 1.17)10^{1}$
K_{CO2} (bar^{-1})	$(6.34 \pm 1.46)10^{-2}$	
K_{H2} (bar^{-1})	$(1.30 \pm 0.87)10^{-2}$	
K_w (bar^{-1})	$(9.11 \pm 1.70)10^{-1}$	

[a] Low significance achieved. Value obtained by a refinement of activation energy provided by Lacerda de Oliveira et al. [33]

One of the most crucial variables in the process is the formation of water during the reaction. Water is formed from CO_2 hydrogenation, but also from methanol conversion to hydrocarbons and its concentration affects the thermodynamics of the reaction, strongly limiting reactions 1 and 2 of the kinetic network (Eqs. (2) and (3)). The evolution of water with the catalytic bed length was simulated at different conditions and its concentration (in mol mol_C^{-1}) is depicted in Fig. 5a. At 350 °C and feeding pure CO_2 (red lines), water concentration shows an asymptotic trend towards 0.4 mol mol_C^{-1} when the reaction is carried out at 30 bar (dashed red line). At 40 bar, due to the evolution of CO_2 conversion, the model no longer predicts the asymptotic trend (solid lines). A maximum value of 0.5 mol mol_C^{-1} can be achieved when increasing the reaction temperature up to 400 °C. This increase in the water concentration with temperature is explained by the promotion of MTH reactions at high temperature. The concentration of water in the reactor can be drastically decreased by co-feeding CO. Considering the asymptotic values at the outlet of the reactor operating at 30 bar (dashed lines), co-feeding 50% CO_2/CO decreases water concentration to 0.2 mol mol_C^{-1}, whereas reaction with pure CO produces a maximum water concentration of 0.05 mol mol_C^{-1}. Again, CO concentration in the feed stream could play an important role in the reaction medium, which should be considered without disregarding the main goal of CO_2 valorization.

Further investigation on the kinetics for these three different feeds were performed. Fig. 5b shows reaction rate values for all steps considered in the kinetic network (Eqs. (2)–(8) and inset of Fig. 5b). Reversible reaction rates are depicted with patterned white bars. At relevant space time values and pure CO_2 feed, CO_2 hydrogenation to methanol, rWGS reaction and CO hydrogenation to methanol are in equilibrium, indicating the hard thermodynamic limitations of the process. These reactions, and especially those involving CO_2, are significantly faster than MTH chemistry at 350 °C (apparent rate also considering hydrocarbon hydrogenation). The rate of CO_2 hydrogenation (reaction 1, blue in Fig. 5b) decreases when co-feeding CO but forward and reverse rates are in equilibrium independently of the feed composition. Nonetheless, the presence of CO in the feed modifies rate distributions. WGS reaction (reverse reaction 2, Eq. (3)) becomes relevant when increasing CO in the feed due to the presence of water in the reaction medium (Fig. 5a), as well as the production of methanol through CO hydrogenation (forward reaction 3, Eq. 4). Consequently, the rate of LPG formation is boosted (up to 4.5 times, Fig. 5b) but the valorization of CO_2 drops. This behavior is better observed following the evolution of CO and CO_2 concentration in the reactor when these two compounds are co-fed (solid symbols and continuous line Fig. 4c). Close to the reactor entrance (low space time), both CO and CO_2 are consumed. However, when the concentration of water is higher and WGS reaction is triggered, CO conversion is boosted and CO_2 concentration increases, which should be avoided in order to maximize CO_2 valorization. Although the rate of LPG formation increases with CO feeds, the rate of undesired methane formation increases even more (up to 5.5 times, Fig. 5b). Methane should be avoided in the CO_2 valorization plant due to separation issues [7].

3.2. CO_2 valorization plant design

Energy considerations were also taken into account for the upscaled reactor simulation. The highly exothermal MTH reaction can potentially

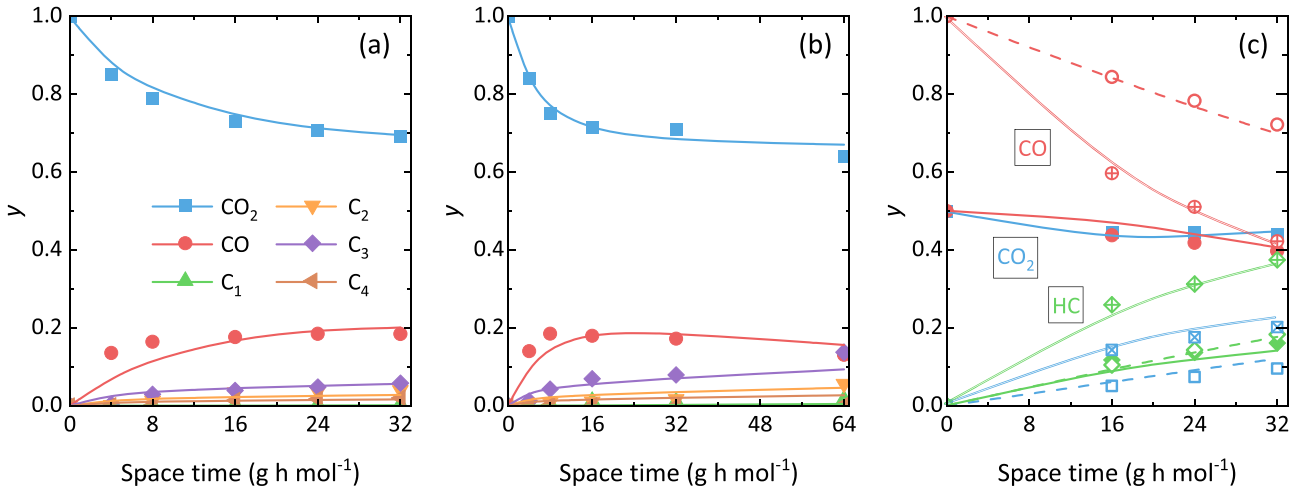

Fig. 4. Comparison of experimental and calculated molar fractions (y on C basis) at 350 °C and (a) 30 bar and (b) 40 bar for pure CO_2 feed. (c) Experimental data fitting with CO in the feed at selected conditions: CO_2/CO = 0.5/0.5, 350 °C and 30 bar (solid symbols and continuous line); CO_2/CO = 0/1, 350 °C and 30 bar (hollow symbols and dashed lines); CO_2/CO = 0/1, 400 °C and 40 bar (crossed symbols and double lines). All data collected with H_2/CO_x = 3/1.

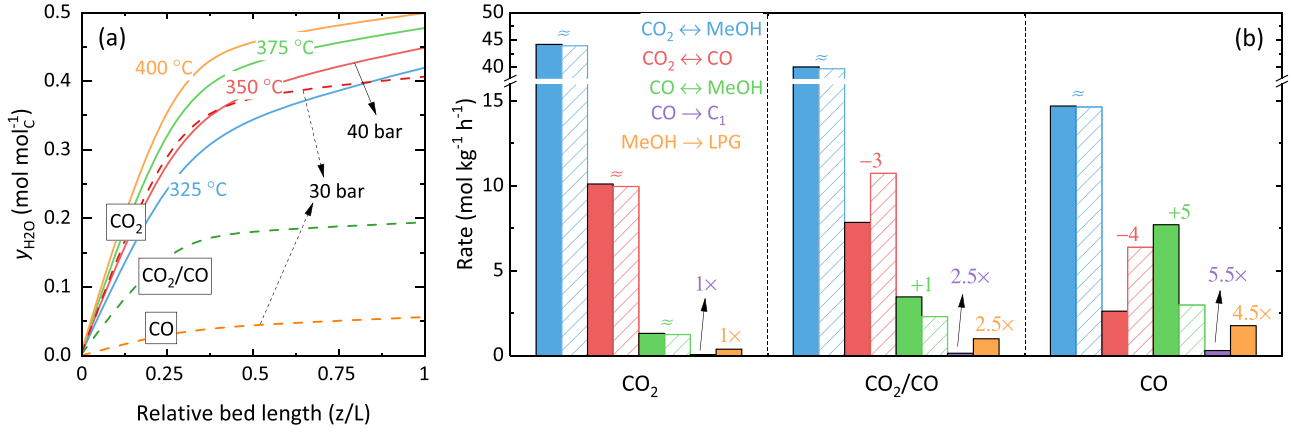

Fig. 5. (a) Effect of temperature, total pressure and CO_2/CO feed concentration on the predicted water profile in the reactor and (b) influence of CO_2/CO feed concentration on the reaction rates at 350 °C, 30 bar. All data computed for space time of 32 g h mol^{-1} (GHSV, 3000 cm^3 h^{-1} g^{-1}) and H_2/CO_x = 3/1.

lead to thermal runaways, which is one of the reasons why this process is industrially carried out using fluidized bed reactors with very high hydrocarbons productivity and heat release [46]. In our case, conditions are quite different for the tandem reaction but the exothermicity of reactions, also CO_2 and CO hydrogenation, limits the maximum allowed diameter of the cooled reactor tubes. An industrial reactor will be therefore designed as a tube bundle reactor. The larger the heat release potential of the reaction, the more measures are required to avoid runaways and the smaller reactor tubes need to be designed (higher number of smaller tubes). Cooling medium is assumed a molten salt, according to the reaction temperature.

To improve the thermal stability and analyze reactor configuration, we herein introduce a multi-layer fixed bed reactor design [47] (Fig. 6a). Here, three layers are used. A first reactor bed is introduced with a pure hydrogenation catalyst ($PdZn/ZrO_2$). Methanol formation reaction rapidly hits equilibrium limitation, with CO being produced through the rWGS reaction and the temperature slightly decreasing due to the endothermic character of this reaction (Fig. 6b). The now reduced heat release potential relaxes the thermal design of the main bed section, where the bifunctional catalyst ($PdZn/ZrO_2$ + SAPO-34) allows the formation and conversion of methanol. This breaks the methanol equilibrium limitation, due to its continuous conversion to LPG. In this section, where mainly exothermal reactions take place, the maximum hot spot is raised (Fig. 6b), which can be better controlled with the presence of the first catalytic bed. Then, to save methanol (and dimethyl ether, DME, which would be inevitably formed and converted in the presence of SAPO-34) losses and avoid extra separation stages, a third bed is included, which only contains MTH catalyst (SAPO-34). Any remaining methanol and DME should be easily converted in this latter section. Fig. 6c shows schematic profiles with the catalytic bed length of temperature and methanol relative concentration in the center of reactor diameter (r/R = 0). Ideally, methanol will be slowly formed in the first section, formed and converted in the second section, and completely removed from the outlet stream in the third section.

The theoretical performance of the three-layer reactor was compared, by means of simulations, to the extreme cases of mixed bed reactor (only using the second section) and dual bed reactor (only using the first and third sections) for the same catalyst loading (Fig. 6c). As an example, 10 wt% of the bed is assumed for the first and third sections, with the mixture of catalysts accounting for 80 wt% of the catalytic bed (10/80/10). Although this ratio should be optimized depending on the operating conditions (temperature, pressure, recirculation/purge ratios, etc.), 10/80/10 was selected as a proper case study that allows a good performance of the reactor in terms of conversion and productivity, ensuring thermal stability and methanol removal downstream. Moreover, a different size of the first and third layers could be used, while we chose to maintain the ratio between the $PdZn/ZrO_2$ and SAPO-34 catalysts in 1:1 (on weight basis) to provide a proper comparison between

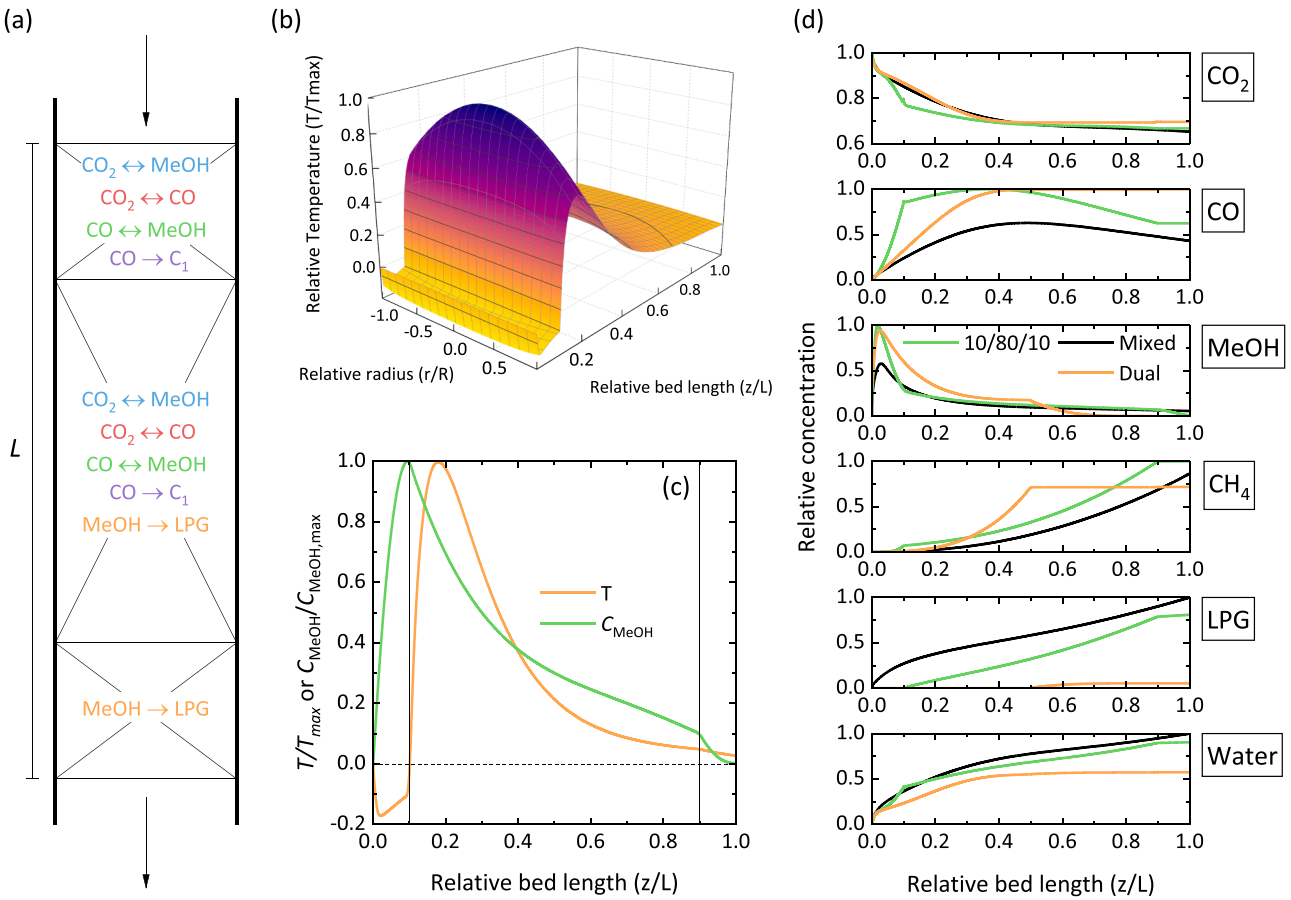

Fig. 6. (a) Approach of the three-layer packed bed reactor, (b) expected temperature profile with the axial and radial position, and (c) estimated temperature profile and methanol concentration with the axial position at $r/R = 0$ (central reactor point). (d) Simulated relative concentration profile with the axial position and different reactor configurations. Corresponding maximum molar fractions in C units (1 in the Y-axis): CO_2, 1; CO, 0.292; MeOH (may contain DME at the outlet of the second zone), 0.061; CH_4, 0.007; LPG, 0.212; water, 0.564 mol mol_C^{-1}.

the configurations.

CO_2 conversion is higher in the mixed bed reactor than that achieved in the dual bed reactor, which is clearly observed in the production of LPG and water. The presence of CO_2 hydrogenation catalyst in the second half of the reactor ($z/L > 0.5$) allows the conversion of CO, decreasing the production of this byproduct per pass and maximizing the formation of LPG and water. Under the operating conditions, methanol reaches productivity maximum very early at any reactor configuration, indicating the necessity of having SAPO-34 in the first half of the reactor ($z/L < 0.5$). A comparison of the mixed bed reactor with the three-layer configuration suggests an overall better performance of the mixed bed reactor. Nonetheless, simulations confirm the presence of a residual amount of methanol (and potentially some DME) at the outlet of the mixed bed reactor (0.5% yield per pass), avoided, as expected, with the three-layer configuration (Fig. 6c). Note that despite the presence of only SAPO-34 in the last layer can produce some unsaturated hydrocarbons, the amount of olefins will be negligible compare to the produced paraffins due to the small amount of methanol after the second reactor layer.

Due to the relevance of water in the reactor and overall process (see below), a similar analysis to that of Fig. 5a can be done for each layer of the reactor. Please note that the water profile of the mixed bed reactor in Fig. 6 (black line) corresponds to an intermediate profile between the red lines (solid and dashed) in Fig. 5a, so then the discussion is applicable. When both catalysts are separated in the dual bed configuration, the formation and effect of water in each layer can be studied separately. In the presence of only $PdZn/ZrO_2$, water concentration increases fast at the beginning as a consequence of CO_2 to methanol reaction (see methanol profile) and keeps increasing only due to the rWGS reaction with lower slope. The presence of water and methanol in this layer limits the CO_2/methanol equilibrium, which affects negatively to the performance of this configuration. Water concentration increases very slowly in the SAPO-34 layer because of the little amount of methanol formed in the first layer and converted very fast here ($0.5 < z/L < 0.7$). Nevertheless, the presence of this formed water, along with the H_2 in the feed helps attenuate the deactivation of SAPO-34, which ultimately allows a packed bed reactor to be used for this process. The three-layer reactor configuration takes better advantage of these water effects, with the presence of water before entering the SAPO-34-containing layer, a continuous conversion of methanol to minimize the equilibrium limitation, and a last section to remove methanol, forming hydrocarbons and small amounts of water ($z/L > 0.9$).

For the simulation of the plant, we have assumed a three-layer reactor (with 10/80/10 catalyst distribution), large enough to achieve CO_x conversion per pass of 50% at 350 °C and 35 bar (optimal found conditions, see above). Although our experimental values are in the 15–40% range (therefore some deviations can be found due to extrapolation), it is not a value very far from our range and will be only used as the basis to compare the performance of the CO_2 valorization plant. Table 2 summarizes the values of the main reaction/process indexes (defined in **Section S1** of Supplementary Material). For this theoretical operation point (50.2% of conversion per pass), an overall CO_x conversion of 95.5% would be achieved, with 90% yield of our desired products and 5.5% yield of methane. However, regarding the weight efficiency of the plant, only 26.1 wt% yield of LPG would be possible with almost 70 wt% yield of water for an overall conversion of 97.7 wt

Table 2
Main process indexes for the CO_2 valorization plant performance.

	C basis		Weight basis	
	Per pass	Plant	Per pass	Plant
Conversion (%, CO_x or $CO_x + H_2$)	50.2	95.5	48.5	97.7
Yields (%)				
CH_4	3.6	5.5	1.1	1.7
LPG	46.6	90.0	13.0	26.1
Water	–	–	34.3	69.9

%. This result highlights again the importance of water separation within the process and the potential high requirement for wastewater (99.9% water) treatment downstream the plant.

Fig. 7 shows the composition of the main streams highlighted in the CO_2 valorization plant of Fig. 1. Fig. 7a shows the molar composition of the streams, whereas the hydrocarbon distribution in terms of C units is detailed in Fig. 7b. The main properties and composition of each stream are summarized in Table S2. As expected, in the steady state, significant amounts of hydrocarbons are recycled to the inlet of the reactor (stream II, ca. 45% in Fig. 7a). This concentration increases after a single pass through the reactor, with a significantly higher increase in water concentration (stream III, 11%). Condensation effectiveness is huge, and only traces of CO_x can be found in the wastewater (stream V). Due to the more difficult separation, ethane and methane are abundant products in the reactor loop of the plant (streams II, III and IV, Fig. 7b), although propane is the main formed hydrocarbon (Fig. 2). The dried hydrocarbon stream (stream VII) has traces of H_2 and CO_x (Fig. 7a) and at this point, propane is clearly the most abundant compound (Fig. 7b), which is further purified in the rectification column up to ca. 80% (stream IX). The secondary product is a mixture of ethane and methane with unseparated propane, and the reactant $H_2/CO_2/CO$ mixture. The main options for this process stream could be combustion, cryogenic separation (e.g. in an existing olefin process) or it can be used as a valuable reformer feed, while the produced synthesis gas is recycled to the process. Considering a non-ideal scenario, we have assumed that this stream will be used for electricity production in our LCA. Regarding these options for the main product streams, the presented process could very well profit from the availability of existing petrochemical plants in an industrial park.

3.3. Life cycle assessment

The results of the CCU plant for LPG production in the three-layer reactor were compared with the impact from the conventional production of propane (Fig. 2b). Based on the functional unit of 1 kg of propane (for the sake of comparison we will use propane as the main component of the produced LPG), the Global Warming Potential results are displayed in Fig. 8a using the current electricity grid mix. For CO_2-based propane, an external source of hydrogen is required, which is included in this study (Fig. 2b). Two different hydrogen sources were considered: (i) grey hydrogen, produced from natural gas *via* steam methane reforming, or; (ii) green hydrogen, produced with clean electricity generating very low greenhouse gas emissions. Two sub scenarios were also considered here, the production of green hydrogen with solar energy or wind energy. Blue hydrogen was not included in the analysis due to high variability of reported fugitive methane emissions and uncertainty in the process data (see assumptions in Section 6 of Supplementary Material). In terms of power-using stages, we considered the compression of the CO_2 and H_2 reactants (Table S4), which was identified as the most demanding step of a CO_2 hydrogenation plant [7]. The evolution of power requirement with the target pressure is depicted in Fig. S6, and the study in Fig. 8a was repeated for an optimized compression system that minimizes power requirement (Fig. S7).

The production of CO_2-based propane (main assumptions highlighted in **Section S6** of the Supplementary Material) would have a lower GWP indicator value than fossil-based propane. Grey hydrogen is currently deployed at commercial scale and would be able to meet an increased demand from carbon reduction projects. In this scenario, the

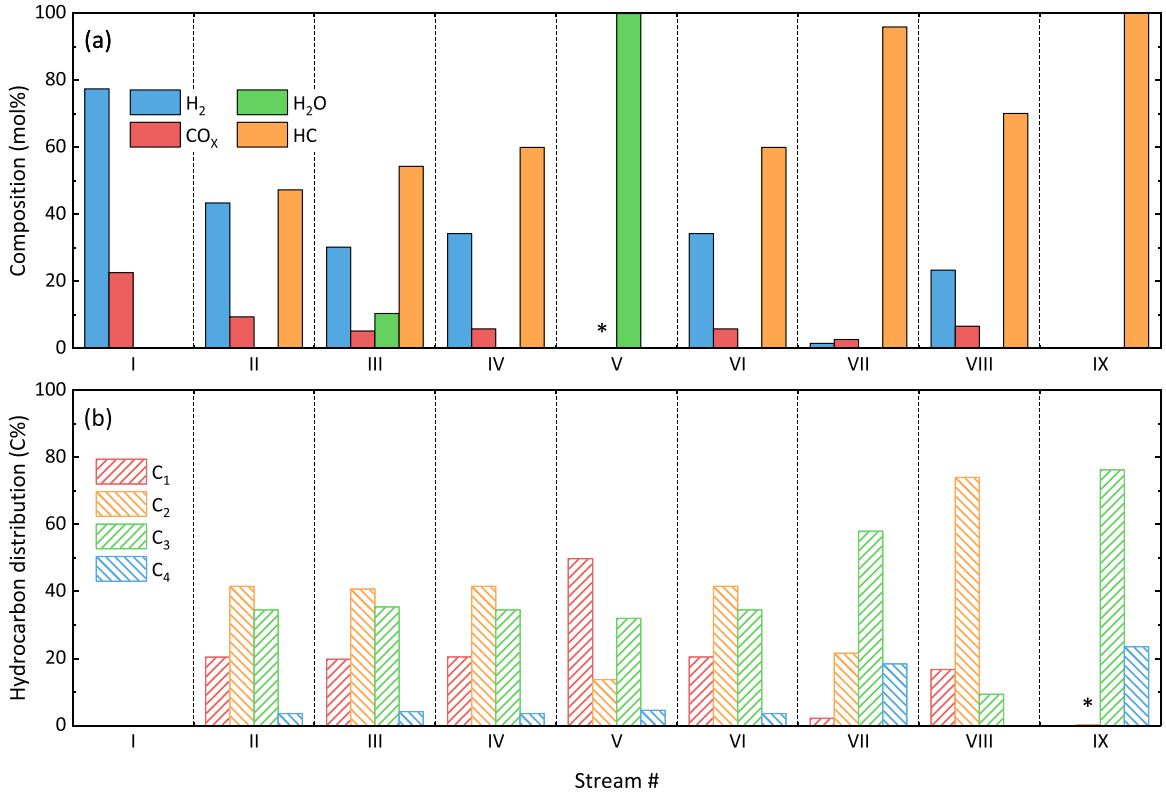

Fig. 7. (a) Molar composition and (b) hydrocarbon distribution of the main streams of the proposed CO_2 valorization plant.

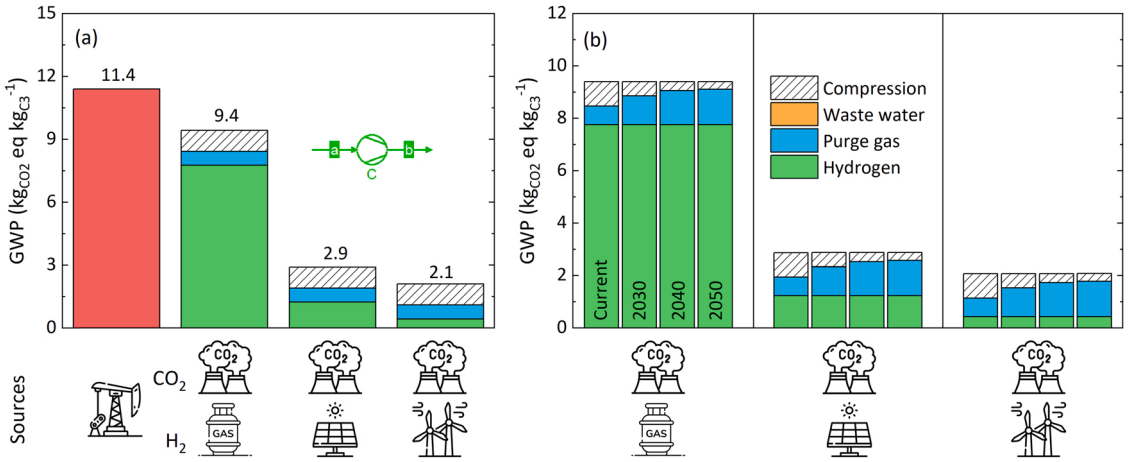

Fig. 8. Comparison of fossil-based propane and CO_2-based propane plant in terms of the GWP indicator and (b) its evolution with time assuming different electricity grid mix scenarios. *All used process data is based on European average, except for electrolysis for the production of hydrogen, which uses global average process data. The GWP of fossil-based propane production was calculated by allocation by mass and net calorific value for all products of the refinery.*

GWP impact would be 18% lower compared to the fossil-based propane, with a carbon footprint of the CO_2-based propane of 9.4 kg CO_2 eq. per kg propane (9.2 kg CO_2 eq. per kg propane for the improved compression scenario, Fig. S7).

The availability of green hydrogen at large scale is still limited. If available, the GWP savings would be significantly increased, to 75% and 82% GWP savings if using green hydrogen from solar energy and wind power respectively (Fig. 8a), compared to fossil-based propane. In these scenarios, the carbon footprint of the CO_2-based propane would be 2.9 and 2.1 kg CO_2 eq. per kg propane, respectively (2.7 and 1.9 kg CO_2 eq. per kg propane for the improved compression scenario, Fig. S7). In the ideal scenario, these two hydrogen sources will be combined, giving GWP indicator values in between those estimated here. The environmental impact is significantly lower in this study when using green hydrogen than those usually reported for a methanol plant [20]. These savings are the consequence of producing propane directly from CO_2 in a single step, as the estimated carbon footprint of producing propane with the current technology (crude oil at refinery) is significantly higher than that of conventional methanol production (natural gas). A breakdown of the impact from the CCU scenario can be observed in Fig. 8a. The hydrogen production accounts for the most significant impact in the CCU process (green blocks in the figure), particularly when using grey hydrogen. Using green hydrogen as opposed to grey hydrogen could further reduce the GWP of the CCU process and the final carbon footprint of the CO_2-based propane. These results are in agreement with most literature [6–12], and urge to maximize the use of green hydrogen and RES in CCU processes. The use of process gases that contain higher amounts of hydrogen would also be highly beneficial. Blast furnace gas only contains 2.7 vol% of H_2. Other industry process gases with higher amounts of H_2 could further decrease the impact of the CCU process.

The effect of using different electricity grid mixes is shown in Fig. 8b. Although the improved compression scenario provides additional savings, a conservative approach is taken in the following figures and the standard compression requirements are used. In line with current trends and predictions, future electricity mixes will have an overall lower GWP impact. The overall GWP impact for each scenario remains almost constant, regardless of the electricity mix considered. As the grid mix is decarbonized, the GWP impact arising from the compression of the input gases is reduced. Regarding the purge gas, the overall impact of combusting purge gas for electricity increases. The emissions of the purge gas depend on its composition and these emissions remain constant. However, when electricity is produced from the purge gas, the applied electricity credit is lower due to the lower emission intensity of the future grid mixes. These results highlight the need to perform full LCA studies of developing technologies and consider any consequential changes like the ones linked to the greening of the grid mix.

To provide a more complete view of the environmental impacts of the CCU plant, a number of impact categories and indicators were studied. The relative results are shown in Fig. 9 for other impacts. The

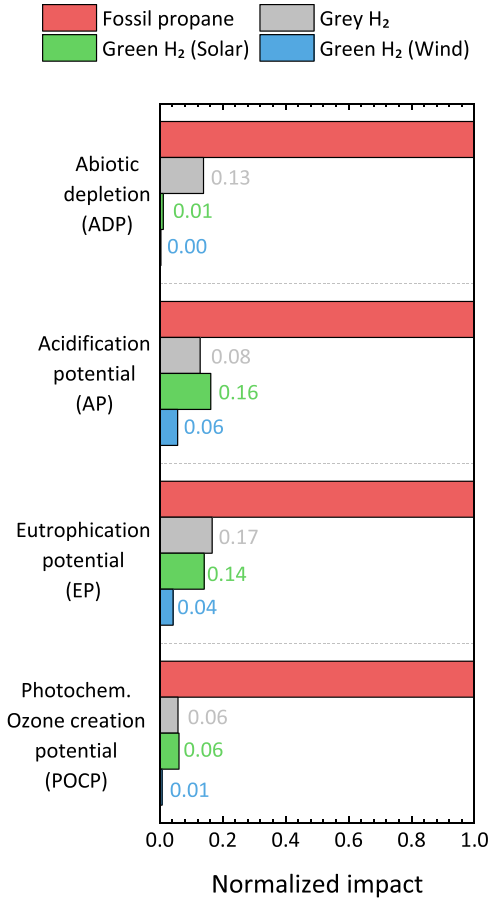

Fig. 9. Comparison of fossil-based propane (red color) and CO_2-based propane using grey H_2 (grey color) or green hydrogen (green and blue colors) in terms of other mid-point indicators. *All used process data is based on European average, except for electrolysis for the production of hydrogen, which uses global average process data. The GWP of fossil-based propane production was calculated by allocation by mass and net calorific value for all products of the refinery.*

results show that in all scenarios considered, the impacts are decreased for abiotic depletion, acidification potential, eutrophication potential and photochemical ozone creation potential. The abiotic depletion of fossil resources is significantly reduced when producing CO_2-based propane as opposed to fossil-based propane. Regardless of the source of hydrogen, every scenario provides a saving compared to the conventional production of propane, from 83% to 100% reduction across the studied impacts. The savings across all impacts are due to the reduced need for fossil resources and the differences in hydrogen source. The differences between the green hydrogen scenarios are linked to the electricity source, solar or wind, which has different implication in material resources needed upstream to generate the electricity.

Despite the certain advantages of CO_2 hydrogenation as CCU technology and the discussed positive environmental impact of propane production compared to the conventional technology, there are still some important points, out of the scope of this work, which are worth considering to implement this technology. The environmental impact of the catalyst has not been considered in this study. To date, one of the most active catalysts we have identified and studied herein for the hydrogenation of CO_2 relies on the high activity of Pd metal [30]. Apart from the expensive price of this metal, whose economic impact would require a cradle-to-gate techno-economic assessment, Pd has also been reported as a metal with high environmental impact. Nuss and Eckelman [48] studied the cradle-to-gate environmental impacts of metals by LCA and found that Pd shows the highest global warming potential after Rh, Pt, Au, Ir and Os, using both mass and economic allocation. Pd can be obtained *via* Platinum group metal ores or by secondary metal production. In the last case, the environmental results are explained by the high environmental impact of the purification process by smelting of electronic scrap. To a smaller degree, the refining process also contributes to the environmental impact. In summary, obtaining Pd would require the use of non-renewable material resources in an industry mainly driven by coal as energy source. These factors boost other environmental mid-point indicators as abiotic depletion if compared to Pd-free catalysts.

Besides related to catalyst requirements, the developed kinetic model considered steady-state conditions and no deactivation based on observations at laboratory scale. There are not that many studies on reactor and/or plant design for the direct conversion of CO_2 to hydrocarbons *via* methanol in a single reactor. Of course, catalyst lifetime in the plant needs to be better assessed, which would require further study and pilot plant experimental results. This information will be useful for the final design of a potential CO_2 valorization plant: type of reactor configuration, reaction-regeneration cycles, reactor shutdown and therefore, catalyst loading to the plant. Ultimately, these features could determine the final and real GWP impact savings of this CCU technology using selected catalysts.

4. Conclusions

Among the Carbon Capture and Utilization technologies, CO_2 hydrogenation is the most developed towards industrial implementation. Herein, the process design, simulation, and Life Cycle Assessment of a CO_2 tandem hydrogenation plant to LPG hydrocarbons *via* methanol is proposed. For that, a state-of-the-art catalyst combination was selected, reactions at a wide range of conditions were carried out and a kinetic model was developed for the CO_2-to-hydrocarbons process. The model successfully predicted the evolution of the product distribution in a packed bed reactor under different conditions (350–400 °C and 20–50 bar), including experiments with only CO feed or cofeeding CO_2 and CO.

Using our extracted kinetics, a reactor model allowed to compare the performance of a three-layer reactor (10% of the bed with CO_2 hydrogenating catalyst, 80% of the bed with a 1:1 mixture of catalysts and 10% of the bed with methanol-to hydrocarbons catalyst) with mixed and dual bed configuration. The three-layer design achieved CO_x conversion and LPG yields close to those predicted for a mixed bed reactor configuration and higher than those values in a dual bed configuration. Moreover, the three-layer design minimized hot-spots close to the reactor entrance and avoided the presence of residual methanol at the outlet of the reactor. Assuming a CO_x conversion per pass of 50 C%, the studied catalyst can convert ca 98 wt% of the CO_2 and H_2 reactants, with 26 wt% yield of LPG but 70 wt% yield of water, as expected from the stoichiometry of the reaction.

The LCA results of the CCU process highlighted that introducing hydrogen into the feed has substantial environmental impact, regardless of the source of hydrogen. With the process described in this study, and assuming that the CCU process uses grey hydrogen, the CO_2-based propane would have an impact of 9.4 kg CO_2 eq per kg of propane. This provides an 18% Global Warming Potential reduction compared to fossil-based propane. The GWP savings can be increased up to 82% if using green hydrogen instead of grey hydrogen. The production of CO_2-based propane also provides significant savings in other impact categories, particularly in the abiotic depletion of fossil resources. A final assessment of the catalyst environmental impact would require further pilot plant results on catalyst performance, stability and lifetime, which will be the goal of our future work. What seems undoubtful is the necessity of more multidisciplinary studies for an optimum development of these new technologies, advancing in parallel into new and more-active catalyst systems and into the process design and LCA to reach real net zero (or negative) CO_2 emissions when using those catalysts.

CRediT authorship contribution statement

Tomás Cordero-Lanzac: Conceptualization, Methodology, Software, Formal analysis, Writing – original draft. **Adrian Ramirez:** Investigation. **Marta Cruz-Fernandez:** Methodology, Formal analysis, Writing – review & editing. **Hans-Jörg Zander:** Methodology, Software. **Finn Joensen:** Investigation, Resources. **Steven Woolass:** Supervision. **Andreas Meiswinkel:** Writing – review & editing, Supervision. **Peter Styring:** Supervision. **Jorge Gascon:** Resources, Writing – review & editing, Supervision. **Unni Olsbye:** Conceptualization, Writing – review & editing, Supervision, Project administration, Funding acquisition.

Declaration of Competing Interest

The authors declare that they have no known competing financial interests or personal relationships that could have appeared to influence the work reported in this paper.

Data availability

Data will be made available on request.

Acknowledgments

This work has been carried out with the financial support of the European Union through the Horizon 2020 research and innovation program under the grant agreement 837733 (COZMOS).

Appendix A. Supporting information

Supplementary data associated with this article can be found in the online version at doi:10.1016/j.jcou.2022.102337.

References

[1] Y. Gu, D. Wang, Q. Chen, Z. Tang, Techno-economic analysis of green methanol plant with optimal design of renewable hydrogen production: A case study in China, Int. J. Hydrog. Energy 47 (2022) 5085–5100, https://doi.org/10.1016/j.ijhydene.2021.11.148.

[2] K. de Kleijne, S.V. Hanssen, L. van Dinteren, M.A.J. Huijbregts, R. van Zelm, H. de Coninck, Limits to Paris compatibility of CO_2 capture and utilization, One Earth 5 (2022) 168–185, https://doi.org/10.1016/j.oneear.2022.01.006.

[3] O. Hoegh-Guldberg, D. Jacob, M. Bindi, S. Brown, I. Camilloni, A. Diedhiou, R. Djalante, K. Ebi, F. Engelbrecht, J. Guiot, Y. Hijioka, S. Mehrotra, A. Payne, S.I. Seneviratne, A. Thomas, R. Warren, G. Zhou, S.A. Halim, M. Achlatis, L.V. Alexander, M. Allen, P. Berry, C. Boyer, E. Byers, L. Brilli, M. Buckeridge, W. Cheung, M. Craig, N. Ellis, J. Evans, H. Fischer, K. Fraedrich, S. Fuss, A. Ganase, J. P. Gattuso, P. Greve, T.G. Bolaños, N. Hanasaki, T. Hasegawa, K. Hayes, A. Hirsch, C. Jones, T. Jung, M. Kanninen, G. Krinner, D. Lawrence, T. Lenton, D. Ley, D. Liverman, N. Mahowald, K. McInnes, K.J. Meissner, R. Millar, K. Mintenbeck, D. Mitchell, A.C. Mix, D. Notz, L. Nurse, A. Okem, L. Olsson, M. Oppenheimer, S. Paz, Petersen, J.J., Petzold, S. Preuschmann, M.F. Rahman, J. Rogelj, H. Scheuffele, C.-F. Schleussner, D. Scott, R. Séférian, J. Sillmann, C. Singh, R. Slade, K. Stephenson, T. Stephenson, M.B. Sylla, M. Tebboth, P. Tschakert, R. Vautard, R. Wartenburger, M. Wehner, N.M. Weyer, F. Whyte, G. Yohe, X. Zhang, R.B. Zougmoré, Impacts of 1.5°C Global Warming on Natural and Human Systems, in: I. Secretariat (Ed.), Glob. Warm. 1.5°C. An IPCC Spec. Rep., 2018: pp. 175–311.

[4] R.M. Cuéllar-Franca, A. Azapagic, Carbon capture, storage and utilisation technologies: A critical analysis and comparison of their life cycle environmental impacts, J. CO_2 Util. 9 (2015) 82–102, https://doi.org/10.1016/j.jcou.2014.12.001.

[5] A. Rafiee, K. Rajab Khalilpour, D. Milani, M. Panahi, Trends in CO_2 conversion and utilization: A review from process systems perspective, J. Environ. Chem. Eng. 6 (2018) 5771–5794, https://doi.org/10.1016/j.jece.2018.08.065.

[6] A.D.N. Kamkeng, M. Wang, J. Hu, W. Du, F. Qian, Transformation technologies for CO_2 utilisation: Current status, challenges and future prospects, Chem. Eng. J. 409 (2021), 128138, https://doi.org/10.1016/j.cej.2020.128138.

[7] T. Cordero-Lanzac, A. Ramirez, A. Navajas, L. Gevers, S. Brunialti, L.M. Gandía, A. T. Aguayo, S. Mani Sarathy, J. Gascon, A techno-economic and life cycle assessment for the production of green methanol from CO_2: catalyst and process bottlenecks, J. Energy Chem. 68 (2022) 255–266, https://doi.org/10.1016/j.jechem.2021.09.045.

[8] S. Sarp, S. Gonzalez Hernandez, C. Chen, S.W. Sheehan, Alcohol production from carbon dioxide: methanol as a fuel and chemical feedstock, Joule 5 (2021) 59–76, https://doi.org/10.1016/j.joule.2020.11.005.

[9] A. Mattos, A. Mitchell, IEAGHG Technical Report. CO_2 Utilisation: Hydrogenation, Pathways (2021).

[10] P. Battaglia, G. Buffo, D. Ferrero, M. Santarelli, A. Lanzini, Methanol synthesis through CO_2 capture and hydrogenation: Thermal integration, energy performance and techno-economic assessment, J. CO_2 Util. 44 (2021), 101407, https://doi.org/10.1016/j.jcou.2020.101407.

[11] F. Lonis, V. Tola, G. Cau, Assessment of integrated energy systems for the production and use of renewable methanol by water electrolysis and CO_2 hydrogenation, Fuel 285 (2021), 119160, https://doi.org/10.1016/j.fuel.2020.119160.

[12] D. Parigi, E. Giglio, A. Soto, M. Santarelli, Power-to-fuels through carbon dioxide Re-Utilization and high-temperature electrolysis: A technical and economical comparison between synthetic methanol and methane, J. Clean. Prod. 226 (2019) 679–691, https://doi.org/10.1016/j.jclepro.2019.04.087.

[13] Emissions-to-Liquids Technology — CRI - Carbon Recycling International, n.d. https://www.carbonrecycling.is/projects#project-goplant (accessed July 29, 2022).

[14] A. Rafiee, Modelling and optimization of methanol synthesis from hydrogen and CO_2, J. Environ. Chem. Eng. 8 (2020), 104314, https://doi.org/10.1016/j.jece.2020.104314.

[15] É.S. Van-Dal, C. Bouallou, Design and simulation of a methanol production plant from CO_2 hydrogenation, J. Clean. Prod. 57 (2013) 38–45, https://doi.org/10.1016/j.jclepro.2013.06.008.

[16] M. Pérez-Fortes, J.C. Schöneberger, A. Boulamanti, E. Tzimas, Methanol synthesis using captured CO_2 as raw material: Techno-economic and environmental assessment, Appl. Energy 161 (2016) 718–732, https://doi.org/10.1016/j.apenergy.2015.07.067.

[17] C. Su, H. Wei, Z. Wang, H. Ayed, A. Mouldi, A.A. Shayesteh, Economic accounting and high-tech strategy for sustainable production: A case study of methanol production from CO_2 hydrogenation, Int. J. Hydrog. Energy 47 (2022) 25929–25944, https://doi.org/10.1016/j.ijhydene.2022.01.124.

[18] T.N. Do, J. Kim, Process development and techno-economic evaluation of methanol production by direct CO_2 hydrogenation using solar-thermal energy, J. CO_2 Util. 33 (2019) 461–472, https://doi.org/10.1016/j.jcou.2019.07.003.

[19] B. Lacerda de Oliveira Campos, K. John, P. Beeskow, K. Herrera Delgado, S. Pitter, N. Dahmen, J. Sauer, A detailed process and techno-economic analysis of methanol synthesis from H_2 and CO_2 with intermediate condensation steps, Processes 10 (2022) 1535, https://doi.org/10.3390/pr10081535.

[20] Y. Khojasteh-Salkuyeh, O. Ashrafi, E. Mostafavi, P. Navarri, CO_2 utilization for methanol production; Part I: Process design and life cycle GHG assessment of different pathways, J. CO_2 Util. 50 (2021), 101608, https://doi.org/10.1016/j.jcou.2021.101608.

[21] S.A. Ning Asih, A. Syauqi, W.W. Purwanto, Techno-enviro-economic analysis of integrated direct chemical looping coal-based power generation and methanol synthesis using renewable hydrogen, J. CO_2 Util. 54 (2021), 101768, https://doi.org/10.1016/j.jcou.2021.101768.

[22] F. Nestler, A.R. Schütze, M. Ouda, M.J. Hadrich, A. Schaadt, S. Bajohr, T. Kolb, Kinetic modelling of methanol synthesis over commercial catalysts: A critical assessment, Chem. Eng. J. 394 (2020), 124881, https://doi.org/10.1016/j.cej.2020.124881.

[23] J. Wang, G. Li, Z. Li, C. Tang, Z. Feng, H. An, H. Liu, T. Liu, C. Li, A highly selective and stable ZnO-ZrO_2 solid solution catalyst for CO_2 hydrogenation to methanol, Sci. Adv. 3 (2017) 1–11, https://doi.org/10.1126/sciadv.1701290.

[24] M.S. Frei, C. Mondelli, A. Cesarini, F. Krumeich, R. Hauert, J.A. Stewart, D. Curulla Ferré, J. Pérez-Ramírez, Role of Zirconia in Indium Oxide-Catalyzed CO_2 Hydrogenation to Methanol, ACS Catal. 10 (2020) 1133–1145, https://doi.org/10.1021/acscatal.9b03305.

[25] A. Bavykina, I. Yarulina, A.J. Al Abdulghani, L. Gevers, M.N. Hedhili, X. Miao, A. R. Galilea, A. Pustovarenko, A. Dikhtiarenko, A. Cadiau, A. Aguilar-Tapia, J. L. Hazemann, S.M. Kozlov, S. Oud-Chikh, L. Cavallo, J. Gascon, Turning a Methanation Co Catalyst into an In-Co Methanol Producer, ACS Catal. 9 (2019) 6910–6918, https://doi.org/10.1021/acscatal.9b01638.

[26] W.H. Feng, M.M. Yu, L.J. Wang, Y.T. Miao, M. Shakouri, J. Ran, Y. Hu, Z. Li, R. Huang, Y.L. Lu, D. Gao, J.F. Wu, Insights into Bimetallic Oxide Synergy during Carbon Dioxide Hydrogenation to Methanol and Dimethyl Ether over GaZrOx Oxide Catalysts, ACS Catal. 11 (2021) 4704–4711, https://doi.org/10.1021/acscatal.0c05410.

[27] P. Tian, G. Zhan, J. Tian, K.B. Tan, M. Guo, Y. Han, T. Fu, J. Huang, Q. Li, Direct CO_2 hydrogenation to light olefins over ZnZrOx mixed with hierarchically hollow SAPO-34 with rice husk as green silicon source and template, Appl. Catal. B Environ. 315 (2022), 121572, https://doi.org/10.1016/j.apcatb.2022.121572.

[28] M. Tong, L. Gapu Chizema, X. Chang, E. Hondo, L. Dai, Y. Zeng, C. Zeng, H. Ahmad, R. Yang, P. Lu, Tandem catalysis over tailored ZnO-ZrO_2/MnSAPO-34 composite catalyst for enhanced light olefins selectivity in CO_2 hydrogenation, Microporous Mesoporous Mater. 320 (2021), 111105, https://doi.org/10.1016/j.micromeso.2021.111105.

[29] J. Mou, X. Fan, F. Liu, X. Wang, T. Zhao, P. Chen, Z. Li, C. Yang, J. Cao, CO_2 hydrogenation to lower olefins over Mn_2O_3-ZnO/SAPO-34 tandem catalysts, Chem. Eng. J. 421 (2021), 129978, https://doi.org/10.1016/j.cej.2021.129978.

[30] A. Ramirez, P. Ticali, D. Salusso, T. Cordero-Lanzac, S. Ould-Chikh, C. Ahoba-Sam, A.L. Bugaev, E. Borfecchia, S. Morandi, M. Signorile, S. Bordiga, J. Gascon, U. Olsbye, Multifunctional Catalyst Combination for the Direct Conversion of CO_2 to Propane, JACS Au 1 (2021) 1719–1732, https://doi.org/10.1021/jacsau.1c00302.

[31] P. Ticali, D. Salusso, R. Ahmad, C. Ahoba-Sam, A. Ramirez, G. Shterk, K. A. Lomachenko, E. Borfecchia, S. Morandi, L. Cavallo, J. Gascon, S. Bordiga, U. Olsbye, CO_2 hydrogenation to methanol and hydrocarbons over bifunctional Zn-doped ZrO2/zeolite catalysts, Catal. Sci. Technol. 11 (2021) 1249–1268, https://doi.org/10.1039/d0cy01550d.

[32] A. Pavlišič, M. Huš, A. Prašnikar, B. Likozar, Multiscale modelling of CO_2 reduction to methanol over industrial Cu/ZnO/Al_2O_3 heterogeneous catalyst: Linking ab initio surface reaction kinetics with reactor fluid dynamics, J. Clean. Prod. 275 (2020), 122958, https://doi.org/10.1016/j.jclepro.2020.122958.

[33] B. Lacerda De Oliveira Campos, K. Herrera Delgado, S. Pitter, J. Sauer, Development of Consistent Kinetic Models Derived from a Microkinetic Model of the Methanol Synthesis, Ind. Eng. Chem. Res. 60 (2021) 15074–15086, https://doi.org/10.1021/acs.iecr.1c02952.

[34] A. Ateka, M. Sánchez-Contador, A. Portillo, J. Bilbao, A.T. Aguayo, Kinetic modeling of CO_2+ CO hydrogenation to DME over a CuO-ZnO-ZrO_2@SAPO-11 core-shell catalyst, Fuel Process. Technol. 206 (2020), 106434, https://doi.org/10.1016/j.fuproc.2020.106434.

[35] T. Cordero-Lanzac, A.T. Aguayo, A.G. Gayubo, P. Castaño, J. Bilbao, A comprehensive approach for designing different configurations of isothermal reactors with fast catalyst deactivation, Chem. Eng. J. 379 (2020), 122260, https://doi.org/10.1016/j.cej.2019.122260.

[36] T. Cordero-Lanzac, A.T. Aguayo, J. Bilbao, Reactor–Regenerator System for the Dimethyl Ether-to-Olefins Process over HZSM-5 Catalysts: Conceptual Development and Analysis of the Process Variables, Ind. Eng. Chem. Res. 59 (2020) 14689–14702, https://doi.org/10.1021/acs.iecr.0c02276.

[37] A.G. Gayubo, A.T. Aguayo, A.E. Sánchez del Campo, A.M. Tarrío, J. Bilbao, Kinetic modeling of methanol transformation into olefins on a SAPO-34 catalyst, Ind. Eng. Chem. Res. 39 (2000) 292–300, https://doi.org/10.1021/ie990188z.

[38] S. Ghosh, J. Sebastian, L. Olsson, D. Creaser, Experimental and kinetic modeling studies of methanol synthesis from CO_2 hydrogenation using In_2O_3 catalyst, Chem. Eng. J. 416 (2021), 129120, https://doi.org/10.1016/j.cej.2021.129120.

[39] I. Iliuta, F. Larachi, P. Fongarland, Dimethyl ether synthesis with in situ H_2O removal in fixed-bed membrane reactor: Model and simulations, Ind. Eng. Chem. Res. 49 (2010) 6870–6877, https://doi.org/10.1021/ie901726u.

[40] VDI Heat Atlas, Springer Berlin Heidelberg, 2010. https://doi.org/10.1007/978–3-540–77877-6.

[41] M.O.S. Dias, A.V. Ensinas, S.A. Nebra, R. Maciel Filho, C.E.V. Rossell, M.R. W. Maciel, Production of bioethanol and other bio-based materials from sugarcane bagasse: Integration to conventional bioethanol production process, Chem. Eng. Res. Des. 87 (2009) 1206–1216, https://doi.org/10.1016/j.cherd.2009.06.020.

[42] S.Y. Oh, M. Binns, H. Cho, J.K. Kim, Energy minimization of MEA-based CO_2 capture process, Appl. Energy 169 (2016) 353–362, https://doi.org/10.1016/j.apenergy.2016.02.046.

[43] CML-IA Characterisation Factors - Leiden University, (n.d.). https://www.universiteitleiden.nl/en/research/research-output/science/cml-ia-characterisation-factors (accessed May 19, 2022).

[44] T. Langhorst, S. McCord, A. Zimmermann, L. Muller, L. Cremonese, T. Strunge, Y. Wang, A. Villa Zaragoza, J. Wunderlich, A. Marxen, K. Armstrong, G. Buchner, A. Kätelhön, M. Bachmann, A. Sternberg, S. Michailos, H. Naims, B. Winter, D. Roskosch, G. Faber, C. Mangin, F. Mason, G. Stokes, E. Williams, B. Olfe-Kräutlein, P. Styring, R. Schomäcker, A. Bardow, V. Sick, Techno-Economic Assessment & Life

Cycle Assessment Guidelines for CO2 Utilization (version 2.0), Global CO2 Initiative, 2022. https://doi.org/10.7302/4190.
[45] T. Shoinkhorova, T. Cordero-Lanzac, A. Ramirez, S.H. Chung, A. Dokania, J. Ruiz-Martinez, J. Gascon, Highly selective and stable production of aromatics via high-pressure methanol conversion, ACS Catal. 11 (2021) 3602–3613, https://doi.org/10.1021/acscatal.0c05133.
[46] P. Tian, Y. Wei, M. Ye, Z. Liu, Methanol to olefins (MTO): From fundamentals to commercialization, ACS Catal. 5 (2015) 1922–1938, https://doi.org/10.1021/acscatal.5b00007.
[47] A. Meiswinkel, H.-J. Zander, Process and plant for producing one or more hydrocarbons, 2021080669, 2021.
[48] P. Nuss, M.J. Eckelman, Life cycle assessment of metals: a scientific synthesis, PLoS One 9 (2014), e101298, https://doi.org/10.1371/JOURNAL.PONE.0101298.